Mon. Not. R. Astron. Soc. **000**, 1–13 () Printed 4 September 2014 (MN LATEX style file v2.2)

X-ray observations of VY Scl-type nova-like binaries in the high and low state

Zemko P.[1⋆]; Orio M.[2,3]†; Mukai, K.[4,5]‡; Shugarov S.[6,7]§
[1] *Department of Physics and Astronomy, Università di Padova, vicolo dell' Osservatorio 3, I-35122 Padova, Italy*
[2] *INAF - Osservatorio di Padova, vicolo dell' Osservatorio 5, I-35122 Padova, Italy*
[3] *Department of Astronomy, University of Wisconsin, 475 N. Charter Str., Madison, WI 53704, USA*
[4] *CRESST and X-ray Astrophysics Laboratory, NASA Goddard Space Flight Center, Greenbelt, MD 20771, USA*
[5] *Department of Physics, University of Maryland, Baltimore County, 1000 Hilltop Circle, Baltimore, MD 21250, USA*
[6] *Sternberg Astronomical Institute, Moscow University, Universitetsky Ave., 13, Moscow 119992, Russia*
[7] *Astronomical Institute of the Slovak Academy of Sciences, Tatranská Lomnica, 059 60, The Slovak Republic*

arXiv:1409.0939v1 [astro-ph.SR] 3 Sep 2014

Accepted . Received ; in original form

ABSTRACT

Four VY Scl-type nova-like systems were observed in X-rays during both the low and the high optical states. We examined *Chandra*, *ROSAT*, *Swift* and *Suzaku* archival observations of BZ Cam, MV Lyr, TT Ari, and V794 Aql. The X-ray flux of BZ Cam is higher during the low state, but there is no supersoft X-ray source (SSS) as hypothesized in previous articles. No SSS was detected in the low state of the any of the other systems, with the X-ray flux decreasing by a factor between 2 and 50. The best fit to the *Swift* X-ray spectra is obtained with a multi-component model of plasma in collisional ionization equilibrium. The high state high resolution spectra of TT Ari taken with *Chandra* ACIS-S and the HETG gratings show a rich emission line spectrum, with prominent lines of in Mg, Si, Ne, and S. The complexity of this spectrum seems to have origin in more than one region, or more than one single physical mechanism. While several emission lines are consistent with a cooling flow in an accretion stream, there is at least an additional component. We discuss the origin of this component, which is probably arising in a wind from the system. We also examine the possibility that the VY Scl systems may be intermediate polars, and that while the boundary layer of the accretion disk emits only in the extreme ultraviolet, part of the X-ray flux may be due to magnetically driven accretion.

Key words: cataclysmic variables – nova-likes: stars.

1 INTRODUCTION

Nova-like (NLs) stars are non-eruptive cataclysmic variables (CVs, see Warner 1995), classified into several subtypes depending on evidence of a strong magnetic field on the white dwarf (WD), and on spectral and photometric characteristics (see Dhillon 1996). Here we will focus on the VY Scl-type nova-likes or 'anti-dwarf' novae characterized by the presence of occasional dips on the light curve, so-called low states, defined by Honeycutt & Kafka (2004) as a fading of the optical light by more than 1.5 mag in less than 150 days. The drop in luminosity can reach 7 mag and may last from weeks to years.

The large optical and UV luminosity seems to imply that the VY Scl-type nova-like, in their longer lasting optically high state, are undergoing mass transfer onto the WD at the high rate $\dot{m} > 10^{-10}$ $M_\odot$ yr^{-1}, sustaining an accretion disk in a stable hot state in which DN outbursts are suppressed (see e.g. the disk thermal instability model of Osaki 2005). The low states have been attributed to a sudden drop of $\dot{m}$ from the secondary, or even to a total cessation of mass transfer (see e.g. King & Cannizzo 1998; Hessman 2000). The reason of this dramatic decrease of $\dot{m}$ is still unclear. The most probable cause may be spots on the surface of the secondary, covering the L1 point and causing the mass-transfer cut off (Livio & Pringle 1994). Wu et al. (1995) have suggested instead non-equilibrium effects in the irradiated atmosphere of the donor.

If the transition from the high to low state occurs because of a decrease in $\dot{m}$, the accretion disks in these systems should move from the equilibrium region to the one of dwarf novae (DN) instabilities, so we should observe

⋆ E-mail:polina.zemko@studenti.unipd.it
† E-mail:marina.orio@oapd.inaf.it
‡ E-mail:koji.mukai@umbc.edu
§ E-mail:shugarov@ta3.sk

(DN) outbursts with recurrence times of 12 to 20 days during the low state, caused by thermal–viscous instabilities in the accretion disk (Warner 1995). However, outbursts in the low state of these objects are extremely rare (see Pavlenko & Shugarov 1999, for MV Lyr). DN outbursts must be suppressed during the low state despite the low $\dot{m}$; this can be explained by a WD effective temperature high enough (30,000–50,000 K) to irradiate the inner accretion disk and maintain it in the stable 'hot' state (Smak 1983), while the incoming mass accretion stream stops or decreases (King 1997; Lasota 1999; Hameury et al. 1999; Leach et al. 1999). The WD in the known DN never reaches this temperature range, but high WD effective temperatures have indeed been inferred via spectroscopic observations in the *UV* and *FUV* ranges for the VY Scl objects (see Table 1). Hameury & Lasota (2002) suggested instead that the DN outbursts are prevented by the periodic disruption of the disc by a magnetic field of the WD, and in this model the VY Scl would be intermediate polars (IP), in which the WD magnetic field is of the order of 10^6 Gauss.

Greiner et al. (1999) proposed a link between the VY Scl-type stars and super soft X-ray sources (SSS) based on a *ROSAT* observations of V751 Cyg. They found an anti-correlation in the optical and X-ray intensity, and despite the very poor spectral resolution of the *ROSAT* HRI, the spectrum appeared to be soft in the low state. The authors suggested that quasi-stable thermonuclear burning occurs on the surface of the WD in the low state, preventing DN outbursts. In this framework, VY Scl stars are key objects in the evolution of interacting WD binaries, in which hydrogen burning occurs periodically without outbursts. Accretion goes on at a very high rate without ever triggering a thermonuclear runaway, because of the recurrent interruptions of the high $\dot{m}$ regime. Thus there is a possibility that VY Scl stars reach the Chandrasekhar mass and the conditions for type Ia supernovae outbursts. Greiner & Teeseling (1998) and Greiner et al. (2001) suggested also thermonuclear burning in the low states of V Sge and BZ Cam. However, these two objects had not been actually observed as SSS; in more recent years an X-ray observation of the VY Scl system V504 Cyg in the low state failed to reveal a luminous SSS (Greiner et al. 2010).

Using archival X-ray observations, in this paper we compare high and low state X-ray data, and some new *UV* data, for four VY Scl-type stars. We seek clues to the complex evolution of these systems, and explanations for the changes that take place during the transition from the high to low state.

2 PREVIOUS OPTICAL AND *UV* OBSERVATIONS

In Table 1 we report parameters from the published results of observations in the optical, near (*NUV*) and far (*FUV*) ultraviolet wavelength ranges. We see that these objects have an orbital period just above the period gap, in a narrow range between 3.2 and 3.7 hours. For the three systems MV Lyr, TT Ari and V794 Aql the WD effective temperature $T_{\rm eff}$ was estimated in previous low states (not shown in Fig. 1) from *UV* and *FUV* observations, in the range between 39,000 K and 47,000 K. These systems could not have been

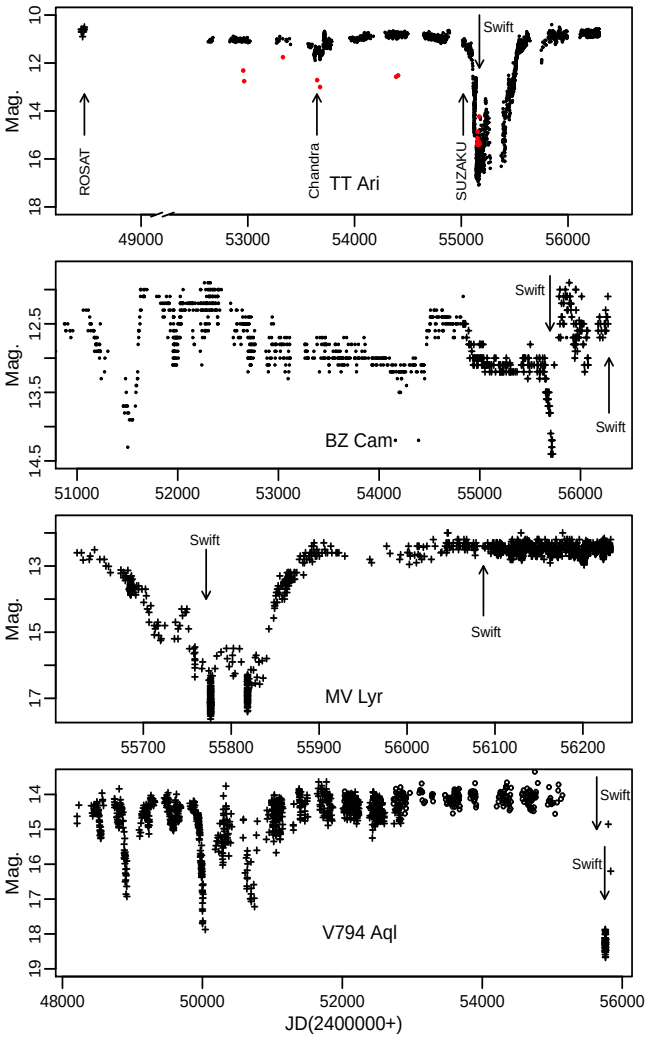

Figure 1. Light curves of TT Ari, BZ Cam, MV Lyr and V794 Aql (from top to bottom) obtained from the AAVSO (crosses), VSNET (filled circles) collaboration and ASAS (open circles) data. The times of the X-ray observations are marked with arrows.

SSS at the time of those observations, because $T_{\rm eff}$ places the flux peak in the *FUV* range. On the other hand, we cannot rule out ignition of thermonuclear burning, neither the possibility that the WD may become hotter with time in subsequent low states. The low state $T_{\rm eff}$ of MV Lyr tabulated in Tab. 1 was measured while the *FUV* flux, corresponding to most of the bolometric one, was about 3.6 $\times 10^{-12}$ erg s^{-1} (see Table 1). In Fig. 5 of Starrfield et al. (2012) we see that at the tabulated distance these values may be consistent with thermonuclear burning with $\dot{m} < 1.6 \times 10^{-10}$ M$_\odot$ yr^{-1} and a WD mass less than 1 M$_\odot$. Godon & Sion (2011) suggested that MV Lyr becomes hotter in the high state, hypothesizing a lower limit $T_{\rm eff} \geqslant 50,000$ K, consistent with a measured *FUV* flux of 2.5 $\times 10^{-10}$ erg s^{-1} in the high state. If the WD really becomes hotter while emitting X-rays at this level, the possibility of thermonuclear burning would be even more likely in the high state. For a WD mass of 0.7 M$_\odot$ and the value of $\dot{m}$ in Table 1, assuming that the extreme *UV* (*EUV*) luminosity is close to the total (bolometric) lumi-

nosity, nuclear burning according to Starrfield et al. (2012) occurs with $T_{\rm eff} \simeq 80,000$ K (see their Fig. 5), which implies a peak luminosity in the *EUV* range and no detectable SSS. An accurate determination of $T_{\rm eff}$ in the high state is important: even an upper limit inferred from the absence of an SSS in the X-rays is useful to constrain the evolutionary models.

3 OBSERVATIONS AND DATA ANALYSIS

We examined the archival X-ray data of VY Scl-type stars obtained with *Swift*, *ROSAT*, *Suzaku* and *Chandra* and chose the objects that were observed both in the high and low states: BZ Cam, MV Lyr, TT Ari and V794 Aql. The data are summarized in Table 2. All the data were never published except for a *ROSAT* observations of TT Ari, which we examined again and which were also analysed by Baykal et al. (1995) and van Teeseling et al. (1996).

In order to assess when the low and high optical states occurred, we relied on the data of the Variable Star Network (VSNET) Collaboration (Kato et al. 2004) [1], the American Association of Variable Star Observers (AAVSO) [2] and ASAS [3] databases. The optical light curves are presented in Figure 1. The epoch of the X-ray observation is marked with an arrow in each plot. We did not find optical data for V794 Aql around the epoch of the X-ray observations taken on 15 March 2011. However, from the photometric observations of the object before and after this date presented in Honeycutt et al. (2014) it is reasonable to assume that V794 Aql was in the intermediate state during the X-ray observation.

We used the HEASOFT version 6-13 to extract the *Swift* and *Suzaku* spectra, and the XSPEC version 12.8.0 for spectral modelling. We also measured the *UV* magnitudes of the objects in both the *Swift*/UVOT observations and in additional *GALEX* archival exposures. The *Chandra* ACIS-S+HETG grating spectra were extracted with CIAO version 4.3. Four different partial exposures were added for both the HEG and MEG gratings spectra with the FTOOL ADDASCASPEC, written originally for *ASCA*, but also useful for all X-ray telescopes and detectors.

For better resolution and in order to use the full exposure, we also combined the data from two *Suzaku* front illuminated detectors (XIS 0 and XIS 3) taken in 3x3 and 5x5 modes. The timing analysis of the *Suzaku* data was performed with the XRONOS sub-package of FTOOLS after the barycentric correction.

4 RESULTS

4.1 TT Ari

TT Arietis is one of the brightest CVs, usually between *V* magnitude 10 and 11. Sometimes it abruptly falls into an 'intermediate state' at $V\simeq14$ or even into a 'low state' reaching $V\simeq18$. According to Belyakov et al. (2010) this binary system consists of a 0.57–1.2 $M_\odot$ white dwarf and a 0.18–0.38 $M_\odot$ secondary component of M 3.5±0.5 spectral type (Gänsicke et al. 1999). The only low state before the one discussed in this paper was observed in the years 1980–1985 (Hudec et al. 1984; Shafter et al. 1985). The first panel of Figure 1 shows the long term light-curve of TT Ari between 1990 and 2013. The optical brightness started declining dramatically at the beginning of 2009 and the low state lasted for about 9 months, with a drop in optical luminosity of about 7 mag. However, in the low state the optical luminosity is not constant, with variations between V=15 and V=18.

The high state X-ray spectrum of TT Ari was at first obtained by *EXOSAT* in Aug 21/22 1985 Hudec et al. (1987). Authors found that the X-ray flux in the range 0.2–4.0 keV was about 1.9×10^{-11} erg cm^{-2} s^{-1}. They also proposed that there are two or more hot emitting X-ray regions and two or more cold absorbing or scattering regions in TT Ari. On January 20 to 21, 1994 TT Ari was also observed with *ASCA* with an effective exposure time $\sim 14,000$ s. Detailed analysis of these data was performed by Baykal & Kiziloğlu (1996). One of the most interesting findings of the previous X-ray observations is the rapid variability of the X-ray flux, a quasi-periodic oscillations (QPO) with a semi-period of 15–26 minutes (Baykal et al. 1995, Baykal & Kiziloğlu 1996). We will show that QPO with periods in this range are observed in all the high state observations we examined. In 2005 the *Chandra* HETG spectra of TT Ari were obtained by C. Mauche (first shown in a presentation by Mauche, 2010). Below we will discuss this set of observations in details.

4.1.1 The X-ray data: the high state

A set of four *Chandra* HETG exposures were obtained within 5 weeks in 2005 (for details see Table 2). In the optical, the source was undergoing a 'shallow decline' from the average optical magnitude in the high state, from $V\simeq10.5$ to $V\leqslant11.5$. Fig. 3 shows the coadded MEG and coadded HEG spectra of four subsequent eposures. There was no significant flux or spectral variability between the different exposures, and we shall describe the coadded MEG and HEG spectra. A rich emission line spectrum was measured, with strong emission lines of Mg, Si, Ne and S.

The strongest lines of the *Chandra* MEG spectrum are listed in Table 3. For the H-like lines we evaluated the flux with a Gaussian fit to the line; we also estimated the flux in the He-like triplet lines (Ne IX, Mg XI, Si XIII), but we could only do it with larger uncertainty because the lines are blended and we needed to fit three Gaussians (note that the intercombination line is not resolved). Moreover, the triplets of He-like lines are observed in a region of the spectrum which is rich in other lines, like those due to transitions of iron. Despite these difficulties, we performed the fit with three Gaussians for the triplets of Si XIII and Mg XI. We added a fourth line of Fe XVIII at 13.509 Å for Ne IX. We thus evaluated the R ratio f/i (intensity of the forbidden to the intercombination line) and the G ratio $\frac{(f+i)}{r}$ (where r is the intensity of the resonance line). We estimated an uncertainty of about 20% on both these ratios. We obtained

[1] http://www.kusastro.kyoto-u.ac.jp/vsnet/
[2] http://www.aavso.org
[3] http://www.astrouw.edu.pl/asas/

Table 1. Binary parameters

	BZ Cam	MV Lyr	TT Ari	V794 Aql
Dist(pc)	830 ± 160[1]	505 ± 50[3]	335 ± 50[7]	690 ± 105[10]
$P_{orb}(d)$	0.1536[2]	0.1329[4]	0.1375[8]	0.1533[11]
i^o	12–40[1]	10–13[4]	17–22[9]	60[10]
$M_{WD}(M_\odot)$		$0.7 \pm 0.1_{(FUV)}$[3]	0.57–$1.2_{(Opt)}$[9]	0.88 ± 0.39[10]
$\dot{m}_{High}(M_\odot\ yr^{-1})$		2–$3\times10^{-9}{}_{(FUV,Opt)}$[5],[6]	$1.1 \times 10^{-8}{}_{(Opt)}$[9]	$10^{-8.5}$–$10^{-8.0}{}_{(FUV)}$[10]
$\dot{m}_{Low}(M_\odot\ yr^{-1})$		$3\times10^{-13}{}_{(Opt)}$[3]	10^{-16}–$10^{-15}{}_{(UV)}$[7]	
$T_{WD\ High}$		$\geqslant 50000K_{(FUV)}$[5]		
$T_{WD\ Low}$		$47000K_{(FUV)}$[3]	$39000K_{(UV)}$[7]	$45000K_{(FUV)}$[10]
$T_{Disk\ Low}$		$< 2500K_{(UV)}$[6]		
$FUV\ Flux_{High}$(erg cm^{-2} s^{-1})		1.4×10^{-10}[5]*	7.8×10^{-10}[12]**	
$FUV\ Flux_{Low}$ (erg cm^{-2} s^{-1})		9.4×10^{-12}[3]**		

Notes:(FUV), (UV), (Opt) – values obtained from Far UV, UV and Optical observations, respectively. * FUV flux was evaluated from the mean continuum level of a spectrum in a rage 910–1190 Å. ** FUV flux was evaluated from the mean continuum level of a spectrum in a rage 920–1180 Å.

[1]Ringwald & Naylor (1998), [2]Patterson et al. (1996), [3]Hoard et al. (2004), [4]Skillman et al. (1995), [5]Godon & Sion (2011), [6]Linnell et al. (2005), [7]Gänsicke et al. (1999), [8]Thorstensen et al. (1985), [9]Belyakov et al. (2010), [10]Godon et al. (2007), [11]Honeycutt & Robertson (1998), [12]Hutchings & Cowley (2007)

Table 2. Observational log of the *ROSAT*, *Swift*, *Suzaku* and *Chandra* observations of VY Scl-type nova-likes that were analysed in this paper.

Name	State	Date	Instrument	Exposure(s)	Count rate (cts s^{-1})
BZ Cam	High	21/12/2012	*Swift*-XRT	15001	0.0720 ± 0.0024
	Low	15/05/2011	*Swift*-XRT	2710	0.100 ± 0.006
MV Lyr	High	08/06/2012	*Swift*-XRT	7569	0.096 ± 0.003
	Low	29/07/2011	*Swift*-XRT	3282	0.039 ± 0.004
TT Ari	High	01/08/1991	*ROSAT*-PSPCB	24464	0.098 ± 0.007
	High	06/09/2005	*Chandra*-HEG	95362*	0.0266 ± 0.0003
	High	06/09/2005	*Chandra*-MEG	95362*	0.0588 ± 0.0005
	High	06/07/2009	*Suzaku*-XIS FI**	28617	0.671 ± 0.003
	High	06/07/2009	*Suzaku*-XIS BI**	28617	0.836 ± 0.005
	Intermediate	16/10/2009	*Swift*-XRT	4421	0.278 ± 0.008
	Low	22/11/2009	*Swift*-XRT	12030	0.0285 ± 0.0019
V794 Aql	Intermediate	15/03/2011	*Swift*-XRT	6148	0.176 ± 0.005
	Low	12/07/2011	*Swift*-XRT	4629	0.055 ± 0.003

*Four observations were taken with *Chandra*-MEG and *Chandra*-HEG on September 6 and October 4, 6 and 9 2005.
** *Suzaku*-XIS FI – are XIS 0 and XIS 3 detectors with front-illuminated (FI) CCDs, while *Suzaku*-XIS BI is the XIS 1 that utilizes a back-illuminated (BI) CCD

R=0.63 and G=0.78 for Ne IX, R=0.36 and G=0.66 for Mg IX, R=0.33 and G=0.66 for Si XIII.

We consulted Porquet & Dubau (2000), who explored the dependence of these ratios on electron density and plasma temperature. The authors assumed a photoionezed plasma, with or without additional collisional ionization. We see from their Figure 8 that the R ratios we obtained corresponds to high density; we obtain a lower limit on the electron density $n_e = 10^{12}$ cm^{-3}, 10^{13} cm^{-3} and $\geqslant 10^{14}$ cm^{-3} for Ne, Mg and Si, respectively. However, it is known that the R ratios appears smaller, as if the density was higher than its actual value, when there is also photoexcitation by a strong UV/EUV source, exciting the f level electrons into the i level (Porquet & Dubau 2000). We do expect additional photoexcitation if the lines are produced very close to the hot and luminous WD of TT Ari, thus, we do not know that in this case the R ratio is a completely reliable indicator. The G ratio, on the other hand, is reliable and indicates plasma temperature $\geqslant 3 \times 10^6$ K, $\geqslant 4 \times 10^6$ K and $\geqslant 7 \times 10^6$ for Ne, Mg and Si, respectively.

The next step was to fit the observed spectra with a physical model. A fit with a plasma in collisional ionization equilibrium is not acceptable because of too high χ^2, but adding a second temperature we obtained a more rea-

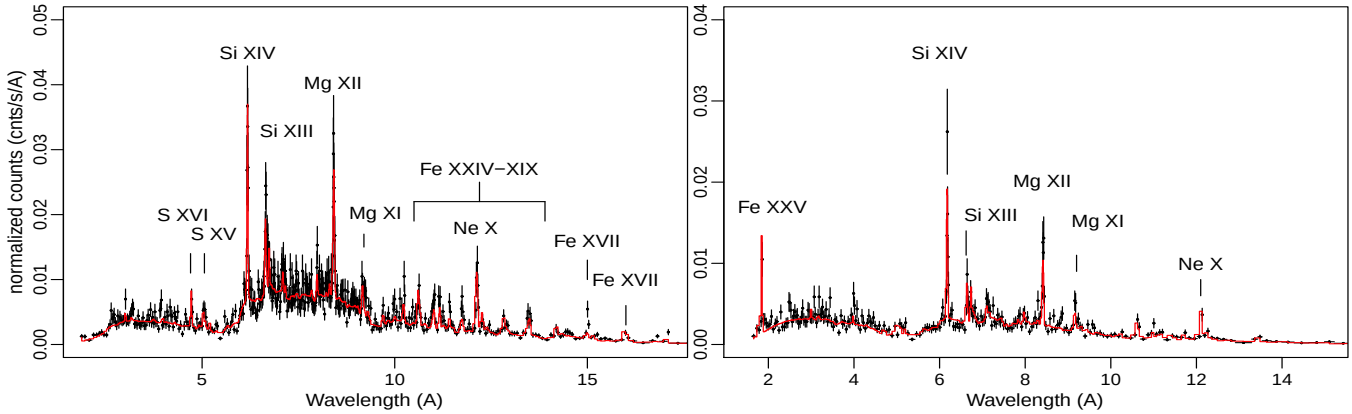

Figure 3. TT Ari spectra observed with the *Chandra* MEG (left) and HEG (right) grating. Four observations and +1 and -1 orders summed. The red lines represent the fit with two VAPEC components. The emission lines are indicated.

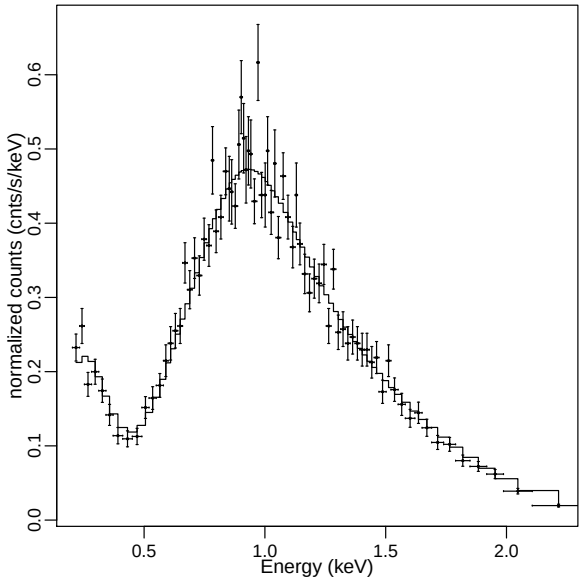

Figure 2. High state X-ray spectrum of TT Ari taken with *ROSAT*.

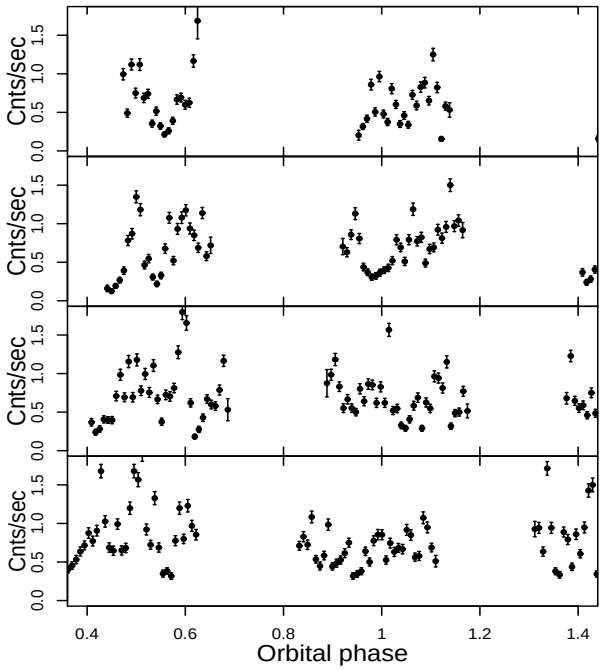

Figure 4. X-ray light curve of TT Ari, obtained by *Suzaku*, binned every 100 seconds. The horizontal axis is the orbital phase. The plots are in chronological order.

sonable fit, with χ^2=1.2. We adopted two BVAPEC models in XSPEC, which describe the emission spectrum of collisionally ionized diffuse gas, calculated using the ATOMDB code v2.0.1 with variable abundances at different temperature (see Table 4 and Fig. 3) and with velocity broadening. By letting the abundances of single elements vary, we found the best fit with the following values for the abundances: [Ne/H]=6.3±1.2, [Mg/H]=4.8±0.8, [Si/H]=4.9±0.9, [S/H]=11 ± 4, [Fe/H]=1.46 ± 0.25, [O/H]=10 ± 4. The emission measure of the cooler component is 3.1×10^{53} cm^3 and the emission measure of the hotter component is 3.6 $\times10^{54}$ cm^3. We note that, if these two regions are related to accretion, for an electron density of order of 10^{14} cm^{-3} (the minimum electron density derived from the G ratio for Si), the linear dimension of the emission region is of order of 3.1 $\times10^8$ cm and 7.1 $\times10^8$ cm, respectively. This is, of course, an purely phenomelogical model; two large and distinct regions with different plasma temperature are difficult to explain in a physically realistic way.

BVAPEC model performs the Gaussian fitting of the lines and gives the σ for two systems of lines associated with the two components (see Table 4). The full width at half maximum that corresponds to these values of σ is about 1100 and 1500 km s^{-1}.

We also wanted to try and better understand the physical scenario by adopting a more physically realistic model. Mukai et al. (2003) have shown that accretion in all non magnetic CVs, and often even in magnetic ones, is best described by a stationary cooling flow model. We thus used the cooling flow VMCFLOW model in XSPEC (a cooling flow model after Mushotzky & Szymkowiak 1988). We see however that this fit yields a larger χ^2 value than the previous simplified model, and this is mainly because there is more

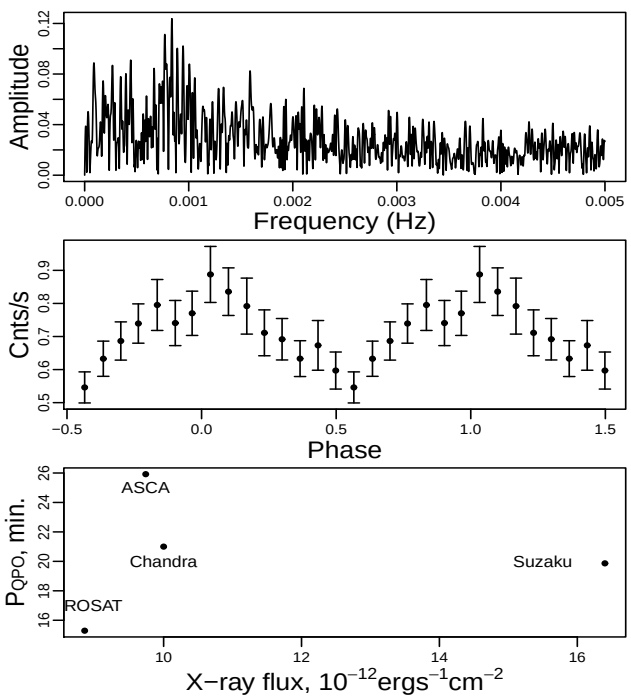

Figure 5. Top panel: the Fourier power spectrum of the *Suzaku* ligh curve of TT Ari. The highest peak corresponds to 0.839 mHz or 19.8 min oscillations. Middle panel: phase folded *Suzaku* light curve with 19.8 min period. Bottom panel: periods of the QPO and flux in the X-ray range 0.5–10.0 keV in the *ROSAT*, *ASCA*, *Chandra* and *Suzaku* observations. We assumed the values of Baykal & Kiziloğlu (1996) for the *ASCA* observations and for the *ROSAT* X-ray flux. The period of the QPO observed with *ROSAT* was taken from Baykal et al. (1995).

flux in the He-like lines than predicted by the model. This may be due to additional photoionization, for instance in a wind from the system, implying that not all the X-ray flux is produced in the accretion flow. The main problem, however, is that the cooling flow model includes the mass accretion rate $\dot{m}$ as a parameter, but predicts a very low value for $\dot{m}$, only 3.48×10^{-11} $M_\odot$ yr^{-1}, while the UV and optical observations indicate 10^{-8} $M_\odot$ yr^{-1} for the high state $\dot{m}$ (see Table 1). We thus conclude that either the observed X-ray flux does not originate in the accretion flow that produces the luminous accretion disk, or that accretion energy is mostly re-radiated in the *EUV* and not in the X-ray range.

The light curves of these *Chandra* exposures still show a QPO, although the modulation has a $\simeq$21 min period. We discuss in detail below the similar light curve we extracted from an additional archival observation done with *Suzaku*, which has higher S/N.

Suzaku observations of TT Ari were obtained by Saitou in 2009 just before the low state (see top panel of Fig. 1). The average X-ray flux during this observation was higher by almost a factor of 2 than during the *Chandra* observation. In order to exclude the effect of a slightly different energy ranges of the detectors we compared the X-ray flux in the range 0.5–10.0 keV, common for both instruments. The difference between the X-ray flux measured with *Chandra* and *Suzaku* may be correlated with the optical one. The *Chandra* HETG observations were taken at the time when TT Ari was optically less luminous ($\geqslant$ 1 mag).

Table 3. Measured wavelength and fluxes in erg cm^{-2} s^{-1} $\times 10^{-14}$ for the emission lines identified in the summed *Chandra* MEG spectrum.

Element	$Energy_{obs}$ (KeV)	λ_{obs} (Å)	MEG $flux^{[1]}_{abs}$
S XV	2.4606^r	5.0387	2.8
	2.448^i	5.064	3.3
	2.4260^f	5.1106	3.4
Si XIV	$2.0061^{+0.0006}_{-0.0010}$	$6.1803^{+0.003}_{-0.0017}$	6.12
Si XIII	1.8650^r	6.6479	3.4
	1.854^i	6.687	1.7
	1.8396^f	6.6739	0.57
Mg XII	$1.4733^{+0.0003}_{-0.0011}$	$8.4154^{+0.006}_{-0.0020}$	3.07
Mg XI	1.3522^r	9.1687	2.0
	1.3434^i	9.2291	1.6
	1.3312^f	9.3136	0.59
Ne X	$1.0211^{+0.0007}_{-0.0004}$	$12.142^{+0.005}_{-0.008}$	5.25
Ne IX	0.9220^r	13.44	3.3
	0.9149^i	13.55	1.8
	0.9051^f	13.69	0.59
Fe XVIII	0.8735	14.19	0.74
Fe XVII	$0.8256^{+0.0004}_{-0.0005}$	$15.017^{+0.008}_{-0.008}$	2.98
Fe XVII	$0.7388^{+0.0006}_{-0.0005}$	$16.781^{+0.014}_{-0.013}$	4.8

[1] For a calculation of fluxes in the lines we assumed N(H)=0.06 $\times$ 10^{22}. r – resonance, i – intercombination and f – forbidden lines.

The broad band spectrum of TT Ari observed with *Suzaku* is presented in Fig. 6. Emission lines of Ne, Mg, Si are clearly seen, like in the *Chandra* spectrum, together with S, Fe XXV, and Fe XXVI lines. We fit this spectrum either with a two-component thermal plasma model with temperatures 0.80 and 7.1 keV (for details see Table 3) and the abundances that were derived from the *Chandra* spectra fit. The residuals of the fit indicate an extra line feature at 6.4 keV in the *Suzaku* spectrum that is most probably the iron fluorescence line. In the inset in Fig. 6 we show the fit of the 5.5–8.0 keV region with three Gaussians at 6.41, 6.68 and 6.96 keV. The equivalent width of the K α iron line at 6.41 keV is 96^{+24}_{-24} eV. This line implies that the X-ray emission region is close to a 'cold' source, which may be the WD surface and/or an optically thick accretion disk, and it is consistent with the WD being less hot than about 100,000 K.

The cooling flow model can be used also for the *Suzaku* spectrum because we do measure spectral lines to constrain the model. The fit is not optimal, and we run into the same problem of low $\dot{m}$.

The *Suzaku* light curve is shown in Fig. 4 and is extremely similar to the light curve previously observed with *ROSAT* (Baykal et al. 1995). The data were integrated in bins of 100 s. The QPO have an amplitude of 50 %. In Fig. 5 we present the Fourier power spectrum of *Suzaku* light curve of TT Ari. The highest peak corresponds to 0.839 mHz or 19.8 min oscillations. According to Andronov et al. (2009) at the time of *Suzaku* observations TT Ari also showed QPO in the optical range, with several peaks, at 2.5, 1.1 and 0.38 mHz. In Baykal et al. (1995) the frequency of QPO in X-ray was explained as the beat frequency between the Kepler

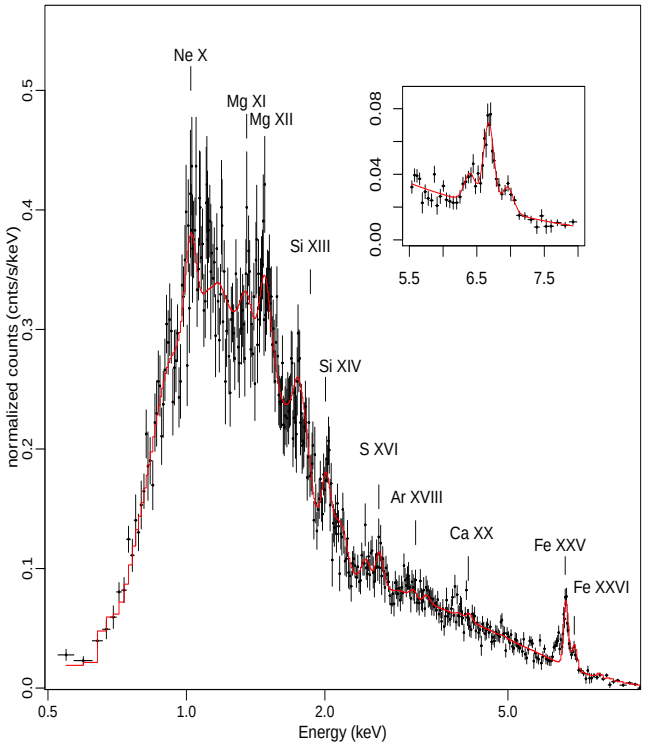

Figure 6. Spectrum observed with the *Suzaku* XIS FI (data from XIS0 and XIS3 detectors taken in 3x3 and 5x5 modes are summed). The red line shows the fit with two VAPEC components. The emission lines are indicated. The inset show the iron K_α emission lines at 6.41, 6.68 and 6.96 keV and their fit with three Gaussians.

frequency at the inner edge of the accretion disk and and the star's rotation rate. Nevertheless, from the QPO semi-periods measured by us in the *Chandra* and *Suzaku* observations and from those derived by Baykal et al. (1995) and Baykal & Kiziloğlu (1996), no correlation emerges between the observed frequency of QPO and the X-ray flux of TT Ari (see the bottom panel of Fig. 5).

In 1991 TT Ari was observed with *ROSAT*. The *ROSAT* X-ray spectrum is shown in Fig. 2. Baykal et al. (1995) analysed these data and found that the best fitting model is an absorbed black-body. We reanalysed the data and found that a black-body can represent only the soft part of the spectrum (the *ROSAT* energy range is 0.2–2.4 keV) and for more sophisticated fit we need two-component thermal plasma model. Parameters of the best fitting model are presented in Table 4.

4.1.2 The X-ray data: the low state

In the intermediate and low state TT Ari was observed with *Swift*. The observations in the intermediate state were presented by Mukai et al. (2009). The unabsorbed flux was about the same as during the *Suzaku* observation, 1.5 $\times 10^{-11}$ ergs cm^{-2} s^{-1}, the spectrum could only be fitted with a multi-temperature plasma, and a new quasiperiod of 0.4 days was also measured in optical.

The low state spectrum, presented in the top panel of Fig. 8, is best fitted with two components of absorbed thermal plasma in collisional ionization equilibrium with a fixed metallicity APEC model at 0.7 keV and 3.9 keV respectively (we only set a fixed metallicity with solar abundances because of the poorer data quality of this dataset). The low state X-ray flux appeared to be about ten times smaller than in the high and intermediate state, and definitely no luminous supersoft X-ray phase was detected. In Table 4 we show also present the comparison with only one component at 3.4 keV. An upper limit to the temperature of a blackbody-like component is approximately 150,000 K.

4.1.3 UV data

In the first panel of Figure 1, in addition to the optical light curve of TT Ari, the red points show the *GALEX* near *UV* (*NUV*) observations. In Table 6 we give exposure times and the mean AB magnitude in the *U*/*UV* filters during the low and high states. The amplitude of the low to high state transition in *NUV* was much lower than in optical: 3 versus 7 magnitudes. Like in the optical range, TT Ari shows flaring activity in the *NUV*, with amplitudes up to 1 mag. However, the *UV* and optical flares occur at different times, and do not appear to correlated, neither anti-correlated. It may be due to the different origine of the *UV* and optical radiation.

4.2 BZ Cam

BZ Cam shows brightness variations around an average value V = 12–13, with rare occasional transitions to low states with V = 14–14.5. Besides the low state studied here, two additional low states were detected – in 1928 and at the beginning of 2000 (Garnavich & Szkody 1988 and Greiner et al. 2001, respectively). BZ Cam is surrounded by a bright emission nebula with a bow-shock structure, first detected by Ellis et al. (1984) and also studied by Krautter et al. (1987), Hollis et al. (1992), Greiner et al. (2001). Hollis et al. (1992) proposed that the bow shock structure is due to the interactions of the wind of BZ Cam with the interstellar medium. The wind in BZ Cam was also studied by Honeycutt et al. (2013). Greiner et al. (2001) suggested that this nebula is photoionized by a bright central object that must be a super soft X-ray source, while the bow shock structure is due to the high proper motion of BZ Cam, moving while it emits the wind.

4.2.1 X-ray data

The second plot of Fig. 8 shows the X-ray spectra of BZ Cam observed with the *Swift* XRT. The luminosity is higher in the low state, however, in the very soft spectral region, at energy $\leqslant$0.5 keV, the X-ray flux is almost twice higher in the high state, which is exactly the opposite of the scenario predicted by Greiner et al. (1999). Interestingly, the spectral fits in both states indicate that we may be observing an unresolved, strong Ne x Lyman α line at 1.02 keV. In the high state spectrum the Fe xxv line at 6.7 keV is clearly detected. BZ Cam was also previously observed with *ROSAT* in the high state. van Teeseling & Verbunt (1994) and Greiner (1998) fitted the spectrum either with one component blackbody or with a highly absorbed bremsstrahlung (or MEWE) model. Greiner (1998) favored the blackbody.

Table 4. Fitting models and parameters for TT Ari. The errors represent 90% confidence region for a single parameter.

	high state					low state	
Satellite	*ROSAT*	*Chandra*		*Suzaku*		*Swift*	
Models	2 apec	2 bvapec	vmcflow	2 vapec+gauss*	vmcflow+gauss*	2 apec	apec
$N(H)_1(10^{22})$	$0.0306^{+0.003}_{-0.0026}$	$0.048^{+0.060}_{-0.048}$	$0.026^{+0.013}_{-0.015}$	$0.136^{+0.022}_{-0.021}$	$0.075^{+0.007}_{-0.010}$	$0.04^{+0.09}_{-0.04}$	$0.019^{+0.05}_{-0.019}$
$N(H)_2(10^{22})$		$0.121^{+0.029}_{-0.029}$					
T_1 (keV)	$0.89^{+0.09}_{-0.11}$	$0.93^{+0.029}_{-0.03}$		$0.80^{+0.13}_{-0.05}$		$0.7^{+0.3}_{-0.4}$	$3.4^{+1.4}_{-0.7}$
T_2 (keV)	25^{+25}_{-13}	$6.5^{+0.5}_{-0.4}$		$7.1^{+0.3}_{-0.3}$		$3.9^{+2.7}_{-1.0}$	
$Sigma_1$ (kms^{-1})		646^{+81}_{-81}					
$Sigma_2$ (kms^{-1})		461^{+119}_{-105}					
EM_1 ($10^{53}cm^{-3}$)**		$3.16^{+0.43}_{-0.26}$					
EM_2 ($10^{53}cm^{-3}$)**		$36.50^{+0.10}_{-0.10}$					
T_{min} (keV)			$0.20^{+0.026}_{-0.026}$		$0.120^{+0.016}_{-0.009}$		
T_{max} (keV)			$21.6^{+1.9}_{-1.4}$		$26.9^{+1.0}_{-1.5}$		
$\dot{m}$ ($\times 10^{-11} M_\odot yr^{-1}$)			$3.36^{+0.27}_{-0.22}$		$5.02^{+0.17}_{-0.11}$		
$Flux^{***}_{abs}$	$5.76^{+0.3}_{-0.13}$	$9.35^{+0.18}_{-0.27}$	$9.01^{+0.011}_{-0.3}$	$15.81^{+0.020}_{-0.020}$	$16.18^{+0.20}_{-0.3}$	$0.99^{+0.17}_{-0.18}$	$0.94^{+0.17}_{-0.18}$
$Flux^{***}_{unabs}$	$6.70^{+0.3}_{-0.13}$	$10.35^{+0.18}_{-0.27}$	$9.21^{+0.011}_{-0.3}$	$17.39^{+0.020}_{-0.020}$	$17.19^{+0.20}_{-0.3}$	$1.08^{+0.17}_{-0.18}$	$1.03^{+0.17}_{-0.18}$
χ^2	1.0	1.2	1.6	1.0	1.2	1.0	1.2

*We added a Gaussian at 6.41 keV in order to fit the Kα iron reflection line in the *Suzaku* spectrum.
**Emission measure
***The X-ray flux ($\times 10^{-12}$erg cm^{-2} s^{-1}) was calculated in the following energy ranges: 0.2–2.5 keV for *ROSAT* PSPC, 0.4–10.0 keV for *Chandra* HETG, 0.5–12.0 keV for *Suzaku* XIS FI and 0.3–10.0 keV for *Swift* XRT

However, with the larger energy range of *Swift* we see that a fit including also the high energy part of the spectrum, is only possible with at least two components, and that the blackbody is not adequate. The black dots in the second panel of Fig. 8 show the low state spectrum of BZ Cam, and a fit with a two-component VAPEC model. With only a broad band spectrum and no detected emission lines, we could not adequately fit the cooling flow model. The same is true for other low resolution X-ray spectra described below.

The high state of BZ Cam (red dots in the second panel of Fig. 8) is best fitted with a two components VAPEC model. The fitting parameters are listed in Table 5. We find the best fit with non solar abundances, [Fe/H]=(4.5 ± 2.4) and [Ne/H]=($\sim$ 14). In the low state, the increased flux seems to be due to a higher maximum temperature, 64 keV instead of about 10 keV. The column density N(H) appears to increase in the low state. Again, a lower limit to the blackbody temperature is of about 150,000 K.

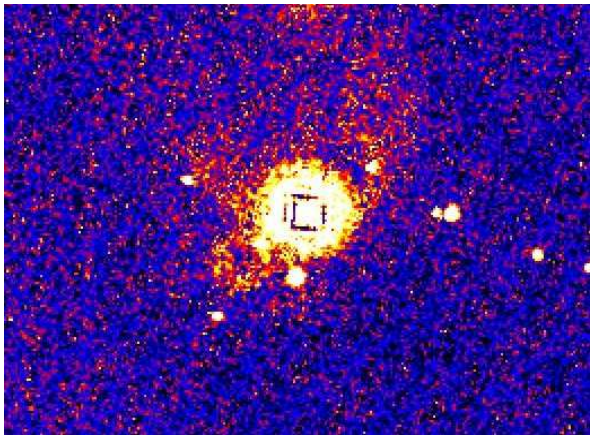

Figure 7. *Swift* UV image of BZ Cam, notice the emission nebula.

4.2.2 UV observations

BZ Cam was observed in *UV* with *Swift* during the low state with a 1172.43 s exposure and with a 121 s exposure during the high state. The UV magnitudes in the AB system in the high and low states, given in Table 6, indicate a smaller variation than observed in the other objects. This is explained by Figure 7 in which we show the UV image of the nebula obtained with *Swift*/UVOT observations. Even with the poor spatial resolution of UVOT, we detect an extended object; obviously the ionized nebula also emits copious UV flux. Comparing the image of BZ Cam in Figure 7 and the optical image in Figure 4 of Greiner et al. (2001), we see a trace of the bow shock oriented in the South-slightly South-West direction, but there seems to be additional *UV* emission of the nebula in the North-East direction, unlike in the in O [III] and H α images taken in September of 2000 with the WIYN telescope (Greiner et al. 2001).

4.3 MV Lyr

MV Lyr spends most of the time in the high state, having brightness in the range V = 12–13, and during the occasional short low states it is in the range V = 16–18. Historical light curves of MV Lyr can be found in Rosino et al. (1993), Wenzel & Fuhrmann (1983), Andronov & Shugarov (1982) and Pavlenko & Shugarov (1998). With their *FUSE* (Far Ultraviolet Spectroscopic Explorer) observations Hoard et al. (2004) estimated that during the low state $\dot{m} \leqslant 3 \times 10^{-13}$ $M_\odot$ yr^{-1}, a four orders of magnitude decrease from the value of $\dot{m}$ estimated by Godon & Sion (2011) in the high state.

Table 5. Fitting models and parameters for BZ Cam and MV Lyr. The errors represent 90% confidence region for a single parameter.

	BZ Cam			MV Lyr		
	high state		low state	high state		low state
Satellite	*Swift*		*Swift*	*Swift*		*Swift*
Models	vapec	2 vapec	2 apec	vapec+plow	2 apec	2 apec
N(H)(10^{22})	$0.14^{+0.03}_{-0.03}$	$0.26^{+0.12}_{-0.08}$	$0.7^{+0.4}_{-0.7}$	$0.24^{+0.5}_{-0.24}$	$0.69^{+0.16}_{-0.26}$	$0.73^{+0.73}_{-0.52}$
Photon Index				$1.00^{+0.5}_{-0.24}$		
T_1 (keV)	$9.3^{+0.2.8}_{-1.7}$	$0.51^{+0.3}_{-0.20}$	$0.3^{+0.0.4}_{-0.3}$	$0.18^{+0.38}_{-0.49}$	$0.11^{+0.03}_{-0.04}$	$0.12^{+0.07}_{-0.05}$
T_2 (keV)		$10.8^{+4}_{-2.3}$	$63.6^{+0.4}_{-54}$		58^{+6}_{-50}	$2.47^{+1.9}_{-1.6}$
$Flux_{abs}$*	$3.85^{+0.24}_{-0.29}$	$4.04^{+0.22}_{-0.3}$	$6.4^{+5}_{-2.2}$	$6.5^{+0.4}_{-1.6}$	$6.0^{+3.5}_{-6}$	$1.2^{+1.3}_{-0.4}$
$Flux_{unabs}$*	$4.24^{+0.24}_{-0.29}$	$4.98^{+0.22}_{-0.3}$	$14^{+5}_{-2.2}$	$9.7^{+0.4}_{-1.6}$	90^{+52}_{-90}	75^{+81}_{-25}
χ^2	1.6	1.1	1.0	1.0	1.2	

*The X-ray flux ($\times 10^{-12}$erg cm^{-2} s^{-1}) for *Swift* XRT was calculated in the range 0.3–10.0 keV

Table 6. UV observations

Object	State	Date	Instrument	Exp.(s)	Mag.$_{AB}$	Filter*
BZ Cam	High	21/12/2012	*Swift* UVOT	1200.74	13.0 ± 1.0	UVW2
	Low	15/05/2011	*Swift* UVOT	2737.32	13.198 ± 0.011	U
MV Lyr	Low	29/07/2011	*Swift* UVOT	2092.81	16.265 ± 0.019	U
TT Ari	High	01/11/2005	*GALEX*	1468.3	12.52 ± 0.001	FUV
	High	13/11/2003–03/11/2007	*GALEX*	80–1686	12.518 ± 0.003	NUV
	Low	15/11/2009–02/12/2009	*GALEX*	1466–1702	15.364 ± 0.003	NUV
	Low	22/11/2009	*Swift* UVOT	6311.28	15.091 ± 0.011	UVW2
V794 Aql	Intermediate	15/03/2011	*Swift* UVOT	6186.67	17.073 ± 0.025	UVW1
	low	12/07/2011	*Swift* UVOT	4732.45	19.26 ± 0.10	UVM2

Swift filters central wavelengths (Å): U – 3465, UVW1 – 2600, UVM2 – 2246, UVW2 – 1928.
GALEX UV band (Å): NUV – 1750–2800, FUV – 1350–1750

4.3.1 X-ray data

The third plot of Figure 8 shows the comparison between the high and low state X-ray spectra of MV Lyr obtained with *Swift* together with the spectral fits. Unlike in BZ Cam, the high state X-ray flux of MV Lyr is higher by an order of magnitude than in the low state. The spectrum is also harder, with an additional component prominent above 1.7 keV.

We fitted the high state spectrum of MV Lyr with a two components thermal plasma model, but a good fit is also obtained with a thermal plasma and a power law model. We fitted the low S/N, low state spectrum with a two components plasma model with fixed solar abundances, without any attempt to explore the role of the abundances (see Table 5).

A *ROSAT* observation of MV Lyr in November 1992 in the high state was studied by Greiner (1998). The authors fitted the spectrum with a black body, however, like in the case of BZ Cam, this model fails to fit the high energy part of the spectrum that we measured with *Swift*. Greiner (1998) observed MV Lyr at the end of the 9 week optical low state in 1996 and obtained only an upper limit for the X-ray luminosity of $10^{29.7}$ erg s^{-1} assuming a distance of 320 pc (smaller than the most current estimate of 505±50 pc we give in Table 1). Assuming a distance of 320 pc, the flux measured during low state observation done with *Swift* (see Tab. 5) four months after the beginning of the decline to the low state, one month after minimum, would be 10^{31} erg s^{-1}, more than a factor of 10 higher than this upper limit. Thus, it seems that the X-ray flux of MV Lyr in the low state is not quite constant.

4.4 V794 Aql

In the high optical state V794 Aql varies between 14th and 15th magnitude, and in the low states it can plunge to 18–20 mag. (in the *B* filter, see Honeycutt & Schlegel 1985). Godon et al. (2007) fitted spectra of the Hubble Space Telescope Space Telescope Imaging Spectrograph (*HST-STIS*) and of *FUSE*. They derived the following binary system parameters: $M_{WD} = 0.9$ M$_\odot$, high state $\dot{M} = 10^{-8.5} - 10^{-8.0}$ M$_\odot$ yr^{-1}, inclination $i = 60^o$, and distance to the system d = 690 pc.

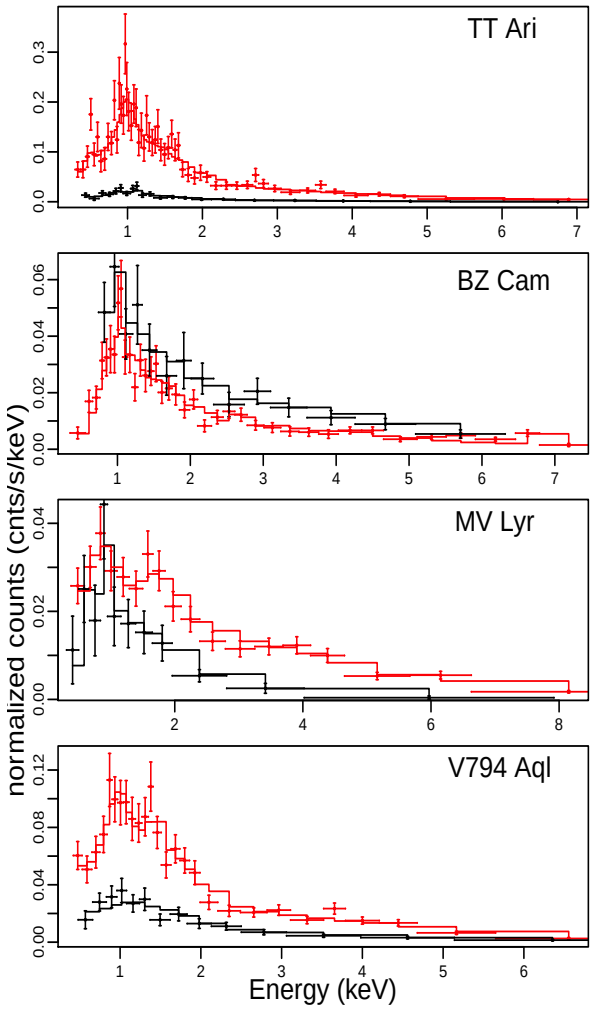

Figure 8. The low and high state X-ray spectra of BZ Cam and MV Lyr observed with *Swift*. TT Ari and V794 Aql were observed with *Swift* during the low and intermediate state. The high and intermediate state spectra are plotted in red and the low state spectra in black. The solid lines show the models, the dots with error bars indicate the data.

4.4.1 The X-ray data

The spectra and their fits of V794 Aql in the intermediate state ($V \simeq 15.5$) and in the low state are presented in the bottom panel of Fig. 8. The X-ray flux is three times higher in the intermediate than in the low state. We fitted the intermediate state spectrum of V794 Aql with two VAPEC components (see Table 7). In both components we need high abundance of Mg (~ 5). Again, there is no luminous supersoft X-ray source in the low state, with an upper limit of about 150,000 K.

5 DISCUSSION

An important motivation for this research has been the claim by Greiner (1998) and Greiner et al. (2001) that some of the WD in VY Scl-type stars must be burning hydrogen quietly in the low state, without ever triggering thermonuclear flashes because of the short duration of the burning. We found that the predicted supersoft X-ray source does not appear in the low states, so thermonuclear burning at high temperature is ruled out. However, as we see in Table 1 at least 3 of the 4 objects we investigated have low mass M_{WD}. According to Starrfield et al. (2012) thermonuclear burning in WDs whose mass is lower than 1 $M_\odot$ occurs quietly with atmospheric temperature below 150,000 K, outside of the SSS window, except for very high values of the mass accretion rate (see Fig.5 of these authors). For Wolf et al. we see that WDs with mass up to 0.7 $M_\odot$ burn hydrogen in the stable regime (without nova eruptions) with $\dot{m}$ of a few times 10^{-7} $M_\odot$ year^{-1} have T_{eff} $\leqslant$200,000 K. We note that also CAL 83, hosting a WD burning H at a much higher atmospheric temperature, has low, intermediate and high states in the optical and X-rays, although with a smaller amplitude in the optical than the VY Scl binaries. These variations were associated with the changes in the amount of irradiation of the accretion disc (see e.g. Greiner & Di Stefano 2002, Rajoelimanana et al. 2013).

Table 7. Fitting models and parameters for V794 Aql. The errors represent 90% confidence region for a single parameter.

	high state	low state
Satellite	*Swift*	*Swift*
Models	2 vapec	apec
N(H)(10^{22})	$0.05^{+0.04}_{-0.03}$	$0.005^{+0.07}_{-0.05}$
T_1 (keV)	$0.9^{+0.3}_{-0.3}$	8^{+20}_{-3}
T_2 (keV)	16^{+39}_{-8}	
$Flux_{abs}$*	$8.2^{+0.5}_{-1.3} \times 10^{-12}$	$2.5^{+0.4}_{-0.6} \times 10^{-12}$
$Flux_{unabs}$*	$8.8^{+0.5}_{-1.3} \times 10^{-12}$	$2.7^{+0.4}_{-0.6} \times 10^{-12}$
χ^2	1.0	0.7

*The X-ray flux ($\times 10^{-12}$erg cm^{-2} s^{-1}) for *Swift* XRT was calculated in the range 0.3–10.0 keV

All the X-ray spectra of the VY Scl systems we examined appear complex, and the *Chandra* and *Suzaku* spectra of TT Ari clearly indicate more than one emission region or mechanism. The best-fitting model for all the 0.3–10.0 keV broad band spectra is a, probably still simplistic, two-component absorbed thermal plasma model. Here we discuss the possible origins of the observed X-ray emission.

5.1 Accretion disk boundary layer

We found that in three of the systems the X-ray luminosity decreases during the optical and UV low states, although the X-ray flux variation is the smallest. The X-ray flux seemed to be anti-correlatd with the optical and UV only in BZ Cam. Thus, if in the other three systems the main source of *UV/FUV* and optical luminosity is the accretion disk, it seems unlikely that the X-ray flux is due to the innermost portion of the disk. In fact, our fits with the cooling flow model, which generally yields good results assuming that all the X-ray flux is emitted in an accretion flow, for all four objects return unreasonably low values of $\dot{m}$, which cannot be reconciled with measurements at other wavelengths. This is not completely unexpected, since the accretion disks of systems accreting at high $\dot{m}$, close to 10^{-8} $M_\odot$ yr^{-1}, seem to re-radiate mostly or completely in the *EUV* range

(Popham & Narayan 1995), because the boundary layer is optically thick.

For TT Ari, the semi-regular variability (QPO) with periods of 17–26 minutes in the high state is best explained with the flickering of an accretion disk, however we also found that there is no correlation between the X-ray flux and the frequency of the QPO, which would be expected for accretion disk flickering (Baykal et al. 1995, Popham 1999).

5.2 X-ray emission in a wind

If the origin of the X-ray emission is not in the boundary layer of the accretion disk, it may originate in a wind, either from the WD or from the accretion disk, depleting matter from the system. Such a wind may play an important role in the evolution, preventing the WD from reaching the Chandrasekhar mass. The fit of the TT Ari emission lines observed with *Chandra* indicates a FWHM in the range 1100–1500 km s^{-1}. However, the lines do not display any measurable blue or red shift to prove a wind scenario. There is significant broadening, but it may be due to collisional ionization in the accretion flow, or to matter in almost-Keplerian rotation. The WD effective temperature and *FUV* flux reported in Table 1 are consistent with a line driven wind, although if nuclear burning takes place, the radius of WD at some stage may increase, and we cannot rule out that at some (still not observed) brief stage the WD reaches a luminosity where also electron scattering opacity starts playing a role (a nova-like radiation pressure wind). In either case, the most likely origin for the X-ray flux in the observations we examined is circumstellar material, shocked when it collides with a new outflow, possibly at a large distance from the WD. There may be circumstellar material left from the AGB phase of primary or old remnant of a previous nova, or a previous 'thicker' wind caused by enhanced luminosity due to nuclear burning, that has slowed down. A strong stellar wind is very likely to play a role in the extended BZ Cam nebula, which was initially classified as a planetary nebula. Instead we would argue that for TT Ari this explanation cannot account for the largest portion of the X-ray flux, because this system shows a 6.4 keV reflection line, which indicates that a large fraction of X-rays (at least X-rays above 7 keV) must originate close to the white dwarf or to the disk.

There is a secure observation of X-rays far away from the accretion disk in UX UMa (see Pratt et al. 2004), an eclipsing nova-like with a hard, absorbed, eclipsed X-ray component and a soft, unabsorbed, uneclipsed X-ray component. The soft X-rays in UX UMa may indeed originate in a wind from the system. A fast wind is also known to occur in CAL 87 (Greiner et al. 2004, Orio et al. 2004), another system that may be closely related to the VY Scl-type stars. The X-rays and optical flux variations anticorrelate only in BZ Cam, so it is possible that in this system the wind increases in the low state, causing additional absorption and obscuring the accretion disk.

Disk winds are observed in many types of compact objects, while the mechanism that causes them is not completely clear. At optical and UV wavelengths a mass outflow from the disk has been inferred in some CV via the observation P Cygni profiles, most notably the C IV λ1549 Å line (Robinson 1973, Cordova & Mason 1982, Long & Knigge 2002). P Cygni line profiles or/and absorption features have also been detected in X-rays in low mass X-ray binaries (Ueda et al. 2001, Brandt & Schulz 2000) and are assumed to originate in a high-velocity outflow from a flared and X-ray-heated accretion disk. Disk winds also cause additional circumstellar, sometimes time-dependent, absorption components in the soft X-rays in non-magnetic CV's (Baskill et al. 2001, Saitou et al. 2012).

5.3 Polar caps

A tempting hypothesis is that, while one component of the X-ray flux is due to a mass outflow from the system, another component originates in a different, and coexistent mode of accretion other than the disk, i.e. a stream to the polar caps. In short, the VY Scl would be intermediate polars (IP's). This scenario explains the lack of a clear correlation of *UV*/optical versus X-ray flux variations. As in the model proposed by Hameury & Lasota (2002) the stream to the polar caps still continue, at decreased rate, when the accretion disk is periodically disrupted in the optically low state. In an IP, the disk would emit in optical and *UV*, but it would be truncated instead of having an X-ray emitting boundary layer, no matter what the value of $\dot{m}$ is.

Mauche (2010) compared spectra of magnetic and non-magnetic CV's and made a point that division into the two classes is not clear-cut on the basis of the X-ray spectrum alone, because of the large variety of observed X-ray spectra of magnetic CV's. There is no 'typical' spectrum among polars and IP's. There is evidence for and against the magnetic scenario for TT Ari, but the X-ray spectrum alone does not prove or disprove it.

An X-ray flux modulation due to the WD rotation period, which is very typical and is considerd the smoking gun to classify IP's, has not been detected in these systems so far. For three of them the reason may be low inclination, but not so for V794 Aql. However, if the major component of the X-ray flux in the high state is not the accretion stream to the poles, but it is associated instead with a wind, isolating the accretion component for the timing analysis is a serious hurdle in detecting a periodicity due to the WD rotation.

6 CONCLUSIONS

The VY Scl binaries are critical to understand the evolution of WD interacting binaries. They pose several riddles for the theories and understanding them well is a key to a consistent evolutionary picture. Are these systems almost always quietly accreting at a high rate, with short intervals of low $\dot{m}$ that prevent the occurence of a thermonuclar flash and mass loss in nova outbursts? Is thermonuclear burning of hydrogen on-going at all phases, and how do we find evidence since we do not observe their WD at the high effective temperature necessary to emit supersoft X-rays?

We analyzed a number of X-rays and UV observations of four VY Scl systems comparing phenomena occurring during the optically 'high' and 'low' state. We did not detect supersoft X-ray emission in both states, however, we cannot exclude H burning at a lower temperature, outside of the SSS window, as can be expected from the low masses of the white dwarfs in these systems. The data collected

and examined in this paper suggest that the X-ray emission has more than one component in all the four systems. We concluded that one component most likely originates in the circumstellar material, shocked by the wind, possibly at a large distance from the WD while the second component can be X-ray emission from the polar caps. However, we are not able to prove neither clearly disprove an IP scenario for these systems.

It can be argued that the X-ray observations at this stage have posed more new puzzles. We suggest that monitoring these systems over the years in optical, *UV* and X-rays as frequently and simultaneously as possible is a key to understand how accretion occurs and how it interplays with the thermal state of the secondary. More intensive monitoring, that may be done with *Swift*, would be very rewarding, allowing to understand whether an evolutionary path at high mass transfer rate without mass loss in nova outbursts can be sustained for a long time, and whether it leads to 'quieter' outflows preventing the WD growth in mass, or to evolution towards a type Ia supernova.

ACKNOWLEDGMENTS

Polina Zemko acknowledges the grant of the National Scholarship Programme SAIA and a pre-doctoral grant of the CARIPARO foundation at the University of Padova. Dr. Shugarov acknowledges the VEGA grant No.2/0002/13.

REFERENCES

Andronov I. L., Baklanov A. V., Liakos A., Niarchos P., 2009, ATEL, 2122
Andronov I. L., Shugarov S. Y., 1982, Astronomicheskij Tsirkulyar, 1218, 3
Baskill D. S., Wheatley P. J., Osborne J. P., 2001, MNRAS, 328, 71
Baykal A., Esendemir A., Kiziloglu Ü., Alpar M. A., Ögelman H., Ercan N., İkis G., 1995, A&A, 299, 421
Baykal A., Kiziloğlu Ü., 1996, Ap&SS, 246, 29
Belyakov K. V., Suleimanov V. F., Nikolaeva E. A., Borisov N. V., 2010, in Werner K., Rauch T., eds, American Institute of Physics Conference Series Vol. 1273 of American Institute of Physics Conference Series, Modeling of the spectral energy distribution of the cataclysmic variable TT Ari and evaluation of the system parameters. pp 342–345
Brandt W. N., Schulz N. S., 2000, ApJ, 544, L123
Cordova F. A., Mason K. O., 1982, ApJ, 260, 716
Dhillon V. S., 1996, in Evans A., Wood J. H., eds, IAU Colloq. 158: Cataclysmic Variables and Related Objects Vol. 208 of Astrophysics and Space Science Library, The Nova-like variables. p. 3
Ellis G. L., Grayson E. T., Bond H. E., 1984, PASP, 96, 283
Gänsicke B. T., Sion E. M., Beuermann K., Fabian D., Cheng F. H., Krautter J., 1999, A&A, 347, 178
Garnavich P., Szkody P., 1988, PASP, 100, 1522
Godon P., Sion E. M., 2011, PASP, 123, 903
Godon P., Sion E. M., Barrett P., Szkody P., 2007, ApJ, 656, 1092
Greiner J., 1998, A&A, 336, 626
Greiner J., Di Stefano R., 2002, A&A, 387, 944
Greiner J., Iyudin A., Jimenez-Garate M., Burwitz V., Schwarz R., DiStefano R., Schulz N., 2004, in Tovmassian G., Sion E., eds, Revista Mexicana de Astronomia y Astrofisica Conference Series Vol. 20 of Revista Mexicana de Astronomia y Astrofisica, vol. 27, Resonant Scattering and Recombination in CAL 87. pp 18–20
Greiner J., Schwarz R., Tappert C., Mennickent R. E., Reinsch K., Sala G., 2010, Astronomische Nachrichten, 331, 227
Greiner J., Teeseling A., 1998, A&A, 339, L21
Greiner J., Tovmassian G., Orio M., Lehmann H., Chavushyan V., Rau A., Schwarz R., Casalegno R., Scholz R., 2001, A&A, 376, 1031
Greiner J., Tovmassian G. H., di Stefano R., Prestwich A., González-Riestra R., Szentasko L., Chavarría C., 1999, A&A, 343, 183
Hameury J.-M., Lasota J., 2002, A&A, 394, 231
Hameury J.-M., Lasota J.-P., Dubus G., 1999, MNRAS, 303, 39
Hessman F. V., 2000, New Astron. Rev., 44, 155
Hoard D. W., Linnell A. P., Szkody P., Fried R. E., Sion E. M., Hubeny I., Wolfe M. A., 2004, ApJ, 604, 346
Hollis J. M., Oliversen R. J., Wagner R. M., Feibelman W. A., 1992, ApJ, 393, 217
Honeycutt R. K., Kafka S., 2004, AJ, 128, 1279
Honeycutt R. K., Kafka S., Robertson J. W., 2013, AJ, p. 45
Honeycutt R. K., Robertson J. W., 1998, AJ, 116, 1961
Honeycutt R. K., Schlegel E. M., 1985, PASP, 97, 1189
Honeycutt R. K., Shears J., Kafka S., Robertson J. W., Henden A. A., 2014, AJ, 147, 105
Hudec R., Huth H., Fuhrmann B., 1984, Observatory, 104, 1
Hudec R., Wenzel W., Goetz W., Valníček B., Peřestý R., Richter G. A., Hacke G., Huth H., Mrkos A., Tremko J., 1987, Ap&SS, 131, 697
Hutchings J. B., Cowley A. P., 2007, AJ, 133, 1204
Kato T., Uemura M., Ishioka R., Nogami D., Kunjaya C., Baba H., Yamaoka H., 2004, PASJ, 56, S1
King A. R., 1997, MNRAS, 288, 16P
King A. R., Cannizzo J. K., 1998, ApJ, 499, 348
Krautter J., Radons G., Klaas U., 1987, A&A, 181, 373
Lasota J.-P., 1999, in Mineshige S., Wheeler J. C., eds, Disk Instabilities in Close Binary Systems Disc and secondary irradiation in dwarf and x-ray novae. Universal Academy Press, p. 191
Leach R., Hessman F. V., King A. R., Stehle R., Mattei J., 1999, MNRAS, 305, 225
Linnell A. P., Szkody P., Gänsicke B., Long K. S., Sion E. M., Hoard D. W., Hubeny I., 2005, ApJ, 624, 923
Livio M., Pringle J. E., 1994, ApJ, 427, 956
Long K. S., Knigge C., 2002, ApJ, 579, 725
Mukai K., Kinkhabwala A., Peterson J. R., Kahn S. M., Paerels F., 2003, ApJ, 586, L77
Mukai K., Patterson J., Koff B., Morelle E., Stein W., Oksanen A., 2009, ATEL, 2254
Mushotzky R. F., Szymkowiak A. E., 1988, in Fabian A. C., ed., NATO ASIC Proc. 229: Cooling Flows in Clusters and Galaxies Einstein Observatory solid state detector observations of cooling flows in clusters of galaxies. pp 53–62

Orio M., Ebisawa K., Heise J., Hartmann J., 2004, in Tovmassian G., Sion E., eds, Revista Mexicana de Astronomia y Astrofisica Conference Series Vol. 20 of Revista Mexicana de Astronomia y Astrofisica, vol. 27, A New View of the Supersoft X-Ray Source Cal 87 Observed with XMM-Newton. pp 210–210
Osaki Y., 2005, Proceeding of the Japan Academy, Series B, 81, 291
Patterson J., Patino R., Thorstensen J. R., Harvey D., Skillman D. R., Ringwald F. A., 1996, AJ, 111, 2422
Pavlenko E. P., Shugarov S. Y., 1998, Astronomical and Astrophysical Transactions, 15, 89
Pavlenko E. P., Shugarov S. Y., 1999, A&A, 343, 909
Popham R., 1999, MNRAS, 308, 979
Popham R., Narayan R., 1995, ApJ, 442, 337
Porquet D., Dubau J., 2000, A&AS, 143, 495
Pratt G. W., Mukai K., Hassall B. J. M., Naylor T., Wood J. H., 2004, MNRAS, 348, L49
Rajoelimanana A. F., Charles P. A., Meintjes P. J., Odendaal A., Udalski A., 2013, MNRAS, 432, 2886
Ringwald F. A., Naylor T., 1998, AJ, 115, 286
Robinson E. L., 1973, ApJ, 186, 347
Rosino L., Romano G., Marziani P., 1993, PASP, 105, 51
Saitou K., Tsujimoto M., Ebisawa K., Ishida M., 2012, PASJ, 64, 88
Shafter A. W., Szkody P., Liebert J., Penning W. R., Bond H. E., Grauer A. D., 1985, ApJ, 290, 707
Skillman D. R., Patterson J., Thorstensen J. R., 1995, PASP, 107, 545
Smak J., 1983, ApJ, 272, 234
Starrfield S., Iliadis C., Timmes F. X., Hix W. R., Arnett W. D., Meakin C., Sparks W. M., 2012, Bulletin of the Astronomical Society of India, 40, 419
Thorstensen J. R., Smak J., Hessman F. V., 1985, PASP, 97, 437
Ueda Y., Asai K., Yamaoka K., Dotani T., Inoue H., 2001, ApJ, 556, L87
van Teeseling A., Beuermann K., Verbunt F., 1996, A&A, 315, 467
van Teeseling A., Verbunt F., 1994, A&A, 292, 519
Warner B., 1995, Cataclysmic Variable Stars. (Cambridge: Cambridge University Press)
Wenzel W., Fuhrmann B., 1983, Zentralinstitut fuer Astrophysik Sternwarte Sonneberg Mitteilungen ueber Veraenderliche Sterne, 9, 175
Wu K., Wickramasinghe D. T., Warner B., 1995, Publ. Astron. Soc. Aust., 12, 60
Mauche, C., 2010, http://*cxc.harvard.edu/cdo/accr*10/*pres*/*Mauche*_Chris.pdf